PNAS RESEARCH ARTICLE | BIOPHYSICS AND COMPUTATIONAL BIOLOGY

Dimerization propensity of the β_1-adrenergic receptor in lipid nanodiscs probed by DEER and single-molecule spectroscopies

Nina Kubatova[a], Thomas Schmidt[a], Quan Wang[a], and G. Marius Clore[a,1]

Affiliations are included on p. 9.

Contributed by G. Marius Clore; received July 21, 2025; accepted August 15, 2025; reviewed by Hashim M. Al-Hashimi, Ilya Kuprov, and David J. Weber

G protein–coupled receptors (GPCRs) comprise a large class of membrane proteins that mediate cellular responses to a wide range of external signals and as such constitute major drug targets. While oligomerization has been shown to play a well-established role in modulating signaling for class C GPCRs (e.g., the glutamate and GABA receptors), the functional relevance of oligomerization for class A receptors, such as the β_1-adrenergic receptor (β_1AR), remains unclear. Here, we have examined the influence of the membrane mimetic environment on the dimerization propensity of β_1AR using a combination of pulsed Q-band double electron–electron resonance spectroscopy and single-molecule fluorescence brightness measurements in an Anti-Brownian Elektrokinetic trap. While β_1AR is predominantly monomeric in docecyl-β-D-maltoside (DDM) micelles, reconstitution of β_1AR in lipid nanodiscs preferentially favors symmetric parallel dimers. Using nanodiscs of different diameters we observed a clear size-dependent increase in the dimer fraction, reaching over 50% of the β_1AR molecules in large (~12.5 nm diameter) nanodiscs. Addition of cholesteryl hemisuccinate, an analog of cholesterol, suppresses β_1AR dimerization in lipid nanodiscs, recapitulating the behavior in DDM micelles. This work provides quantitative evidence that β_1AR possesses an intrinsic, membrane sensitive predisposition for dimerization, and highlights the importance of spatial membrane constraints in the modulation of class A GPCR dimerization.

GPCR | double electron–electron resonance EPR | single molecule ABEL trap | dimerization | nanodiscs

G protein–coupled receptors (GPCRs) constitute a large group of cell surface receptors comprising 7 transmembrane helices and, as such, have been a major focus of pharmaceutical research (1–3). Several studies have linked GPCR oligomerization to ligand binding and subsequent G-protein activation (4–7). However, with the exception of class C GPCRs (that include glutamate and GABA receptors), oligomerization appears to be receptor-specific and remains poorly understood. Demonstrating the existence and functional relevance of GPCR oligomers has been hindered by numerous technical challenges (8). Further, the majority of in vitro studies have been performed under conditions that favor the monomeric form (9, 10). One of the central challenges in studying membrane proteins is their dependence on the lipid environment to maintain native structure and function. While live cells or cell-derived membranes provide the most physiologically relevant context, these systems are limited by heterogeneity, lack of experimental control, and constraints on available experimental methods. To overcome these limitations, various membrane-mimicking systems have been developed for in vitro GPCR studies (11). Among them, lipid nanodiscs offer a powerful platform: they consist of self-assembled phospholipid bilayers stabilized by two membrane scaffold proteins (MSPs), allowing precise control over membrane size and composition (12, 13). The diameter of nanodiscs typically ranges from 7 to 16 nm, enabling the reconstitution of one or more GPCRs [~3 nm diameter for the transmembrane core (14)] within a single nanodisc, and are therefore particularly well suited for investigating oligomerization (15).

Adrenergic receptors are members of the class A (rhodopsin-like) family of GPCRs, the largest and most diverse family of GPCRs (3, 16), and respond to catecholamines such as adrenaline and noradrenaline (17). Adrenergic receptors regulate heart rate, blood pressure, and metabolism, and, hence, are prominent drug targets in the treatment of hypertension, asthma, and heart failure. The β_1-adrenergic receptor (β_1AR) is predominantly expressed in cardiac tissue and plays a critical role in regulating cardiac output. Activation of β_1AR stimulates the sympathetic nervous system, modulating cardiovascular function. Dysregulation of β_1AR leads to a variety of diseases involving the heart (18).

Significance

Despite extensive structural studies of G protein–coupled receptors (GPCRs), the oligomerization properties of class A GPCRs, such as the β_1-adrenergic receptor (β_1AR), remain elusive. Most in vitro studies have been conducted in detergent micelles, which may obscure intrinsic oligomerization tendencies. Using double electron–electron resonance spectroscopy and single-molecule brightness measurements, we show that β_1AR preferentially forms symmetric parallel dimers in lipid nanodiscs but remains predominantly monomeric in micelles. Dimerization is influenced by nanodisc size and inhibited by cholesteryl hemisuccinate. These findings provide insights into how membrane composition and physical constraints regulate GPCR assembly, and suggest that β_1AR dimerization may be controlled in native membranes, a factor that may be critical for understanding receptor function and therapeutic targeting of dimer-specific signaling pathways.

Author contributions: N.K., T.S., Q.W., and G.M.C. designed research; N.K., T.S., and Q.W. performed research; N.K., T.S., Q.W., and G.M.C. analyzed data; and N.K., Q.W., and G.M.C. wrote the paper.

Reviewers: H.M.A., Columbia University; I.K., Weizmann Institute of Science; and D.J.W., University of Maryland, Baltimore.

The authors declare no competing interest.

[1]To whom correspondence may be addressed. Email: mariusc@mail.nih.gov.

This article contains supporting information online at https://www.pnas.org/lookup/suppl/doi:10.1073/pnas.2519609122/-/DCSupplemental.

Published September 18, 2025.

Symmetric dimers of rhodopsin—the most prominent example of the class A GPCR family—have been previously observed in native membranes by atomic force microscopy (19) and in lipid nanodiscs by cryoelectron microscopy (20). For both β_1AR and its close relative the β_2-adrenergic receptor (β_2AR), dimers in cell membranes have been observed by bioluminescence resonance energy transfer (BRET) (21–23). The heterogeneous membrane composition of living cells, however, may impact GPCR oligomerization preferences (24).

Here, we used a combination of Q-band pulsed EPR-based double electron–electron resonance (DEER) (25, 26) and single-molecule fluorescence brightness measurements in an Anti-Brownian Elektrokinetic (ABEL) trap (27, 28) to examine the effect of the membrane mimicking system, specifically lipid nanodiscs, on the oligomeric preferences of β_1AR. DEER measures pairwise distances up to ~60 Å between spin-labeled sites in nondeuterated frozen proteins (26) allowing detection of conformational states or oligomerization at angstrom-level resolution. Single-molecule fluorescence and electrokinetic trapping measures both brightness and diffusion of individual molecules in solution, permitting monomers to be distinguished from dimers in real time at room temperature. Measurements were carried out for two different sizes of lipid nanodiscs, MSP1D1 (diameter ~9.2 nm) and MSP1E3D1 (diameter ~12.5 nm) (12). Both DEER spectroscopy and single-molecule fluorescence brightness measurements show that β_1AR exists predominantly in a monomeric state in *n*-dodecyl-β-D-maltoside (DDM) micelles, but preferentially forms dimers when incorporated into nanodiscs. The dimer population is correlated with the diameter of the nanodiscs. Incorporation of cholesteryl hemisuccinate (CHS), an analog of cholesterol, into the nanodiscs suppresses dimerization of β_1AR, consistent with previous observations in DDM micelles (29).

Results and Discussion

Membrane-Mimicking Systems. To investigate the effect of membrane-mimicking systems on β_1AR oligomerization, we compared DDM micelles, one of the most commonly used GPCR environments (30, 31), with lipid nanodiscs which provide a more native-like membrane-mimicking system for in vitro experiments (32). Two DMPC lipid nanodiscs with different diameters, governed by the chosen MSP, were used in the current work: namely small MSP1D1 and large MSP1E3D1 nanodiscs with respective diameters of ~9.2 and 12.5 nm (*SI Appendix*, Fig. S1). β_1AR was incorporated into the small nanodiscs at ratios of β_1AR-to-nanodiscs of 1:4 and 1:1 and into large nanodiscs at ratios of 1:10, 1:4, and 2:1 (Table 1). The size of the large MSP1E3D1 nanodiscs is known to be sufficient to readily accommodate two GPCR molecules (15, 33). To ensure pure β_1AR-nanodisc samples, it was essential to separate empty nanodiscs from β_1AR containing nanodiscs. To this end we made use of a β_1AR construct with a second histidine tag at the C-terminus, positioned before the 3C protease cleavage site (34), thereby enabling β_1AR containing nanodiscs to be purified by nickel affinity chromatography.

Table 1. Component ratios used for β_1AR reconstruction in nanodiscs

Nanodisc	β_1AR	MSP:β_1AR	Nanodisc: β_1AR	DMPC:MSP
MSP1D1	1	8	4	85
MSP1D1	1	2	1	85
MSP1E3D1	1	20	10	160
MSP1E3D1	1	8	4	160
MSP1E3D1	2	2	1	120

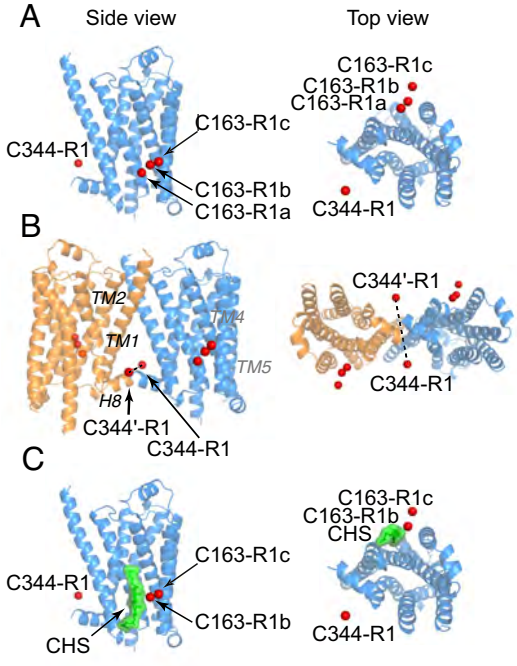

Fig. 1. β_1AR structures. (*A*) Monomeric β_1AR (PDB 2Y00) (38); (*B*) dimeric β_1AR (PDB 4GPO) (36); (*C*) β_1AR in complex with CHS (PDB 2Y00) (38). The sites of R1 nitroxide spin-labeling at Cys163 and Cys344, calculated from the molecular coordinates with the CalcPr helper function in Xplor-NIH (39) are shown as red spheres (29). CHS is displayed as a green space-filling model. Note that C163-R1 occupies three distinct rotamers in the absence of CHS; in the presence of CHS, however, C163-R1 occupies only two distinct rotamers, owing to displacement of one of the rotamers by bound CHS (29). The β_1AR dimer shown in panel B corresponds to the dimer orientation found in rhodopsin (19) and the dimer interface is formed by transmembrane helices TM1 and TM2 and the C-terminal helix H8 (36); the dimer interface is stabilized by hydrophobic and van der Waals interactions; in addition Ser45 and Ser45′ in TM1 for an intermolecular hydrogen bond, and there is a salt bridge between Glu41 (TM1) of one subunit and Arg104 (TM2) of the other (36). This figure has been adapted from figure 2 of Kubatova et al. (29) published in Proc. Natl. Acad. Sci. U.S.A. while the authors were U.S. Government employees at the NIH.

R1-Nitroxide Labeling, DEER, and Basis Set *P*(*r*) Distributions for Pure β_1AR Monomer and Dimer. In our previous work we showed that only two cysteines, C163 and C344, are labeled with the R1 nitroxide (29). β_1AR is largely monomeric in DDM (Fig. 1*A*); addition of cholate promotes dimerization (Fig. 1*B*), while addition of CHS favors the monomeric state (Fig. 1*C*) (29). In DDM and DDM/cholate, C163-R1 exists in three distinct rotameric states giving rise to three intrasubunit distances at 31, 34, and 39 Å between C163-R1 and C344-R1 observed by DEER (Fig. 2 *B* and *C*) (29, 35). In addition, one intersubunit distance between C344-R1 and C344′-R1 is observed by DEER at 26 Å which serves as a reporter of the symmetric parallel dimer (Fig. 2*B*) (29) whose interface is formed by transmembrane helices TM1 and TM2 and the C-terminal helix H8 (36). [In a biologically spurious antiparallel dimer the C344-R1–C344′-R1 distance would be in excess of 80 Å (29); similarly, in an alternative biologically irrelevant dimer interface formed by transmembrane helices TM4 and TM5 (36), the intermolecular distances between spin labels are too long and inconsistent with the DEER data (29).] Note that the monomer and dimer peaks in the *P*(*r*) distribution can be differentiated by T_1-edited DEER as the T_1 values for a dimer are approximately half those of a monomer owing to a doubling of the number of nitroxide labels within the molecular entity of interest (35). Since β_1AR was not deuterated, one cannot assume that all the peaks in the *P*(*r*) distance distribution are characterized by the same phase memory relaxation time (37); that is one cannot

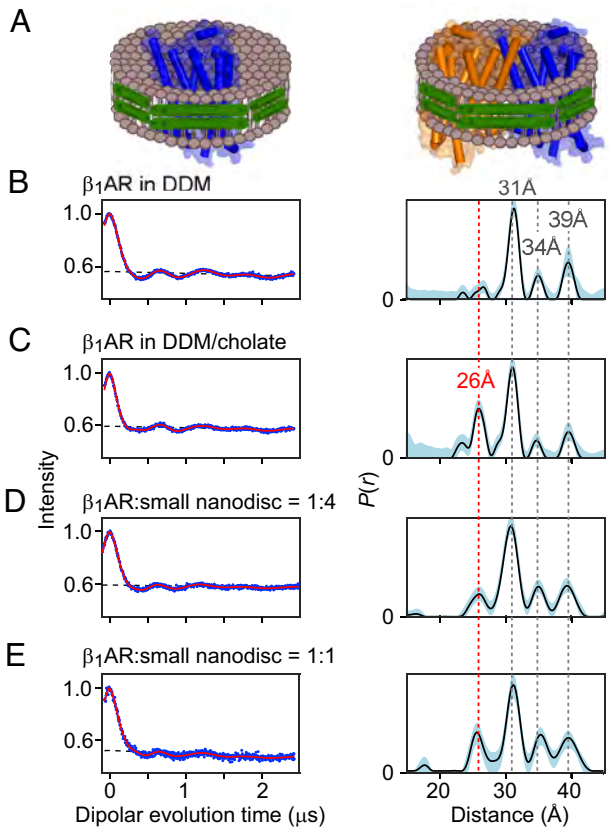

Fig. 2. Q-band DEER measurements on nitroxide spin-labeled β_1AR (C163-R1/C344-R1) in small MSP1D1 nanodiscs. (*A*) Diagrammatic representation of monomeric (blue, *Left* panel) and dimeric (*Right* panel; with one subunit in blue and the other in orange) β_1AR incorporated into small (9.2 nm diameter) MSP1D1 lipid nanodiscs. The MSP1D1 proteins are shown in green. DEER echo-curves (*Left*) and corresponding *P*(*r*) distance distributions (*Right*) for (*B*) β_1AR in DDM micelles, (*C*) β_1AR in DDM micelles with 50.5 mM cholate; (*D*) β_1AR in small nanodiscs at a ratio of β_1AR-to-nanodiscs of 1:4; (*E*) β_1AR in small nanodiscs at a ratio of β_1AR-to-nanodiscs of 1:1. The experimental DEER echo curves (blue) and the corresponding best-fit curves obtained by validated Tikhonov regularization (40) are shown in the left-hand panels of (*B–E*). The exponential background functions are shown as dashed lines. The corresponding *P*(*r*) distance distributions obtained by validated Tikhonov regularization are shown in the *Right*-hand panels of (*B–E*) as black lines with the light blue shading indicating the upper and lower confidence limits. The data in panels (*B*) and (*C*) are reproduced from figure 2 *A* and *C* of Kubatova et al. (29) published in Proc. Natl. Acad. Sci. U.S.A. while the authors were U.S. Government employees at the NIH.

assume that for a pure dimer, the intensity of the intersubunit 26 Å peak is half that of the sum of the intensities of the intrasubunit 31, 34, and 39 Å peaks. Hence, to determine the percentage dimer present from the DEER-derived *P*(*r*) distribution, one needs to determine the basis set *P*(*r*) distributions for the pure dimer and the pure monomer. This was previously done by T_1-edited DEER using the same duration of the dipolar evolution time as in the current work ($T = 2\tau_2 = 6$ μs): For the pure monomer, the fractions of the 31, 34, and 39 Å peaks are 0.57, 0.16, and 0.26, respectively; for the pure dimer, the fractions for the 26, 31, 34, and 39 Å peaks are 0.46, 0.38, 010, and 0.08, respectively (35). The same pure monomer and dimer basis set *P*(*r*) distributions, within experimental error, are also obtained from global analysis of the DEER data obtained for β_1AR in DDM upon titration with cholate (29).

To determine the fractions of the 26, 31, 34, and 39 Å peaks for the β_1AR samples in DDM and DDM/cholate, we fit the DEER-derived *P*(*r*) distributions obtained by Tikhonov regularization (Fig. 2 *B* and *C*) to a sum of four Gaussians centered at these four peak positions. With the *P*(*r*) distributions for pure monomer and dimer in hand, we calculate that the percentages of dimer molecules present in the β_1AR samples in DDM and DDM/cholate are 17% and 66%, respectively, with 5 to 95% confidence limits of 16 to 18% and 57 to 77%, respectively (Table 2).

DEER of β_1AR in Small MSP1D1 Nanodiscs. A schematic of a β_1AR monomer and dimer embedded in a small MSP1D1 nanodisc is depicted in Fig. 2*A*. Given the diameters of the MSP1D1 nanodisc (9.2 nm) and transmembrane core of a β_1AR monomer (~3 to 3.5 nm), one can deduce that the space available for a β_1AR dimer (diameter ~ 7.5 nm) within a small nanodisc is rather limited and would therefore tend to disfavor incorporation of a β_1AR dimer. However, even at a β_1AR-to-nanodisc ratio of 1:4, the DEER-derived *P*(*r*) distribution indicates that ~30% of the β_1AR molecules incorporated into the small nanodiscs are dimeric (Fig. 2*D* and Table 2). At a β_1AR-to- nanodisc ratio of 1:1 the DEER-derived *P*(*r*) distribution shows that the percentage dimer is further increased to ~40% (Fig. 2*E* and Table 2). Since the percentage β_1AR dimer in DDM micelles is small (<20%), one can therefore conclude that, despite steric restrictions imposed by the small diameter of the MSP1D1 nanodiscs, the β_1AR parallel dimer is preferentially incorporated into nanodiscs and enriched during reconstruction. Further, it is important to bear in mind that incorporation of β_1AR into nanodiscs during reconstruction

Table 2. Percentage β_1AR dimer under various membrane-mimicking conditions determined by DEER and single-molecule fluorescence brightness*

Conditions	Percentage β_1AR dimer molecules	
	DEER	Single-molecule brightness
	(5 to 95% limits)	Lower bound estimate
DDM micelles		
β_1AR in DDM	17 (16 to 18)	11
β_1AR in DDM/cholate	66 (57 to 77)	
β_1AR in DDM/CHS	6 (4 to 8)	
MSP1D1 small (9.2 nm) nanodiscs		
β_1AR:nanodiscs = 1:4	31 (25 to 37)	17
β_1AR:nanodiscs = 1:1	38 (29 to 49)	
MSP1E3D1 large (12.5 nm) nanodiscs		
β_1AR:nanodiscs = 1:10	44 (36 to 54)	
β_1AR:nanodiscs = 1:4	65 (56 to 76)	44
β_1AR:nanodiscs = 2:1	57 (52 to 62)	50
MSP1E3D1 large (12.5 nm) nanodiscs + CHS		
β_1AR:MSP1E3D1:CHS = 1:4:700		22
β_1AR:MSP1E3D1:CHS = 2:1:100	14 (8 to 20)	
β_1AR:MSP1E3D1:CHS = 2:1:700	0	

*The DEER data specifically detect the symmetric parallel dimer depicted in Fig. 1*B* (whose interface is formed by transmembrane helices TM1 and TM2 and the C-terminal helix H8) and characterized by a 26 Å intermolecular distance between the unpaired electrons of C344-R1 of one subunit and C344-R1′ of the other (29). In contrast, the single molecule brightness measurements count fluorescent labels per particle and are therefore not sensitive to the type of dimer (parallel vs. antiparallel) but simply to the number of β_1AR monomer units present in a nanodisc (which may also include multiple β_1AR monomers in random orientations); further the single molecule data only provide a lower bound estimate of the dimer population due to potential incomplete labeling and photobleaching.

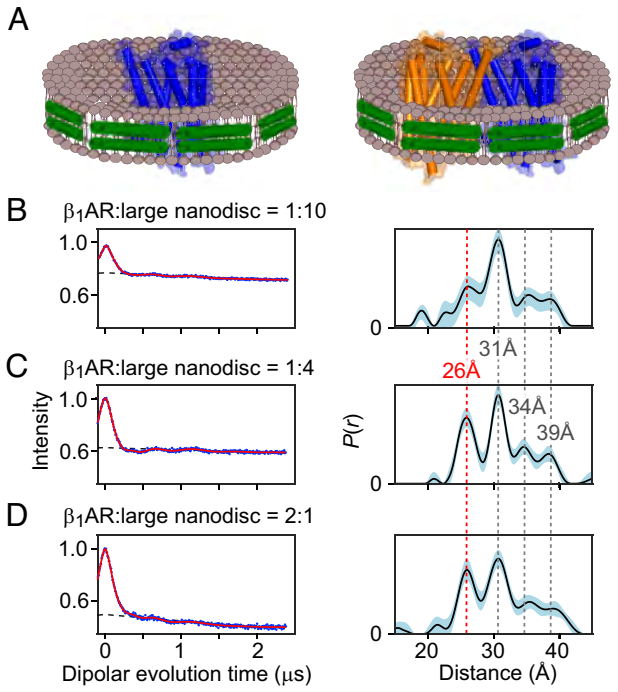

Fig. 3. Q-band DEER measurements on nitroxide spin-labeled β_1AR (C163-R1/C344-R1) in large MSP1E3D1 nanodiscs. (*A*) Diagrammatic representation of monomeric (blue, *Left* panel) and dimeric (*Right* panel; with one subunit in blue and the other in orange) β_1AR incorporated into large (12.5 nm diameter) MSP1E3D1 lipid nanodiscs. The MSP1E3D1 proteins are shown in green. DEER echo-curves (*Left*) and corresponding *P*(*r*) distance distributions (*Right*) for β_1AR incorporated into large nanodiscs at ratios of β_1AR-to-nanodiscs of (*B*) 1:10, (*C*) 1:4 and (*D*) 2:1. The experimental DEER echo curves (blue) and the corresponding best-fit curves obtained by validated Tikhonov regularization (40) are shown in the left-hand panels of (*B*) and (*C*). The exponential background functions are shown as dashed lines. The corresponding *P*(*r*) distance distributions obtained by validated Tikhonov regularization (40) are shown in the *Right*-hand panels of (*B*) and (*C*) as black lines with the light blue shading indicating the upper and lower confidence limits.

involves an effectively irreversible process. That is to say, while one can envisage an equilibrium between monomeric and dimeric β_1AR in DDM micelles involving transient fusion of micelles, no such equilibrium can exist between nanodiscs with monomeric β_1AR and nanodiscs with dimeric β_1AR, since β_1AR cannot simply transition from one nanodisc to another without precipitating out of solution and two nanodiscs cannot fuse with one another. Indeed, an attempt to further increase the incorporation of β_1AR dimer into small nanodiscs by raising the β_1AR-to-nanodisc ratio above 1:1 resulted in sample precipitation, suggesting that while the small nanodiscs can stretch to accommodate some dimers, the small nanodiscs lack the structural capacity to provide a fully relaxed environment for β_1AR dimers.

DEER of β_1AR in Large MSP1E3D1 Nanodiscs. A schematic of a β_1AR monomer and dimer embedded in a large MSP1E3D1 nanodiscs is depicted in Fig. 3*A*. The diameter of 12.5 nm for the MSP1E3D1 nanodiscs (*SI Appendix*, Fig. S1) can easily accommodate a dimer of β_1AR with no steric hindrance. We therefore reasoned that the fraction of β_1AR molecules incorporated in the dimeric form should be significantly enhanced relative to the smaller MSP1D1 nanodiscs. The DEER echo curves and corresponding *P*(*r*) distributions at β_1AR-to-nanodisc ratios of 1:10, 1:4, and 2:1 are shown in Fig. 3 *B*, *C*, and *D*, respectively. Even at a β_1AR-to-nanodisc ratio of 1:10, where one would expect almost all reconstituted β_1AR to be monomeric in the absence of preferential incorporation of β_1AR dimer, ~44% of the reconstituted β_1AR molecules are dimeric (Fig. 3*B* and Table 2). Increasing the β_1AR-to-nanodisc ratio to 1:4 results in maximal dimer incorporation of ~65% (Fig. 3*C* and Table 2), and no further increase in the percentage of incorporated dimer (~57%) is observed at a β_1AR-to-nanodisc ratio of 2:1 (Fig. 3*D* and Table 2). Indeed, the percentage dimer is slightly reduced (albeit not significantly) at the 2:1 ratio, possibly due to precipitation of unincorporated β_1AR during the reconstitution process.

Effect of CHS on β_1AR Dimerization in Nanodiscs. Cholesterol, a key component of eukaryotic cell membranes, modulates the function, dynamics, and oligomerization behavior of GPCRs (41, 42). In the case of β_1AR, cholesterol is a negative allosteric modulator reducing conformational flexibility and impeding access to the active state of the receptor (43). Due to its poor aqueous solubility, cholesterol is frequently substituted by CHS in structural and biophysical studies (29). CHS binds to the cholesterol consensus motif (CCM) cleft formed by transmembrane helices TM2–4 (44). The spin-labeling site C163-R1 is positioned near the CCM binding pocket (Fig. 1*C*), making it an ideal probe for studying the interaction of CHS with β_1AR by DEER spectroscopy (29). Indeed, one of the three rotamers of C163-R1 is displaced upon addition of CHS, resulting in the disappearance of the 31 Å peak and leaving two intrasubunit distances at 34 and 39 Å in the DEER-derived *P*(*r*) distribution (Fig. 4*A*) (29).

To investigate the effect of CHS on β_1AR dimerization in large MSP1E3D1 nanodiscs, we employed two different experimental approaches. In the first, CHS was dissolved in DMPC and incorporated directly during nanodisc reconstitution. In this instance, the highest achievable CHS-to-β_1AR ratio was 100, limited by the solubility of DMPC (Fig. 4*B*). In the second, CHS was dissolved in DDM and added to β_1AR solubilized in DDM micelles prior

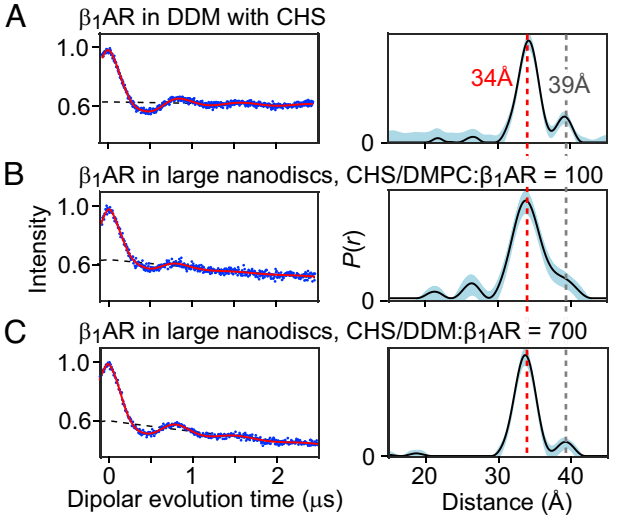

Fig. 4. Q-band DEER measurements on nitroxide spin-labeled β_1AR (C163-R1/C344-R1) in the presence of CHS reconstituted in DDM micelles or large (12.5 nm diameter) MSP1E3D1 nanodiscs. (*A*) β_1AR in DDM at a β_1AR-to-CHS ratio of 1:700. (*B* and *C*) β_1AR incorporated into large (12.5 nm diameter) MSP1E3D1 nanodiscs at a 2:1 ratio of β_1AR-to-nanodiscs with either (*B*) CHS dissolved in DMPC lipids prior to nanodisc reconstruction and added at a β_1AR-to-CHS ratio of 1:100, or (*C*) CHS dissolved in DDM prior to nanodisc reconstruction and added at a CHS-to-β_1AR ratio of 1:700. The experimental DEER echo curves (blue) and the corresponding best-fit curves obtained by validated Tikhonov regularization (40) are shown in the *Left*-hand panels with the exponential background functions represented as dashed lines. The corresponding *P*(*r*) distance distributions obtained by validated Tikhonov regularization (40) are shown in the *Right*-hand panels as black lines with the light blue shading indicating the upper and lower confidence limits. The data in panel *A* are reproduced from figure 3*A* of Kubatova et al. (29) published in Proc. Natl. Acad. Sci. U.S.A. while the authors were U.S. Government employees at the NIH.

to nanodisc reconstitution. This method allows CHS to interact with the receptor in the micellar phase and enables the use of much higher CHS-to-β_1AR ratios: the CHS-to-β_1AR ratio employed was 700:1 and represents a saturated CHS concentration in DDM micelles. In both cases, the ratio of β_1AR-to-nanodisc was 2:1, providing the most favorable conditions for the incorporation of two β_1AR molecules per nanodisc.

The DEER echo curves and corresponding $P(r)$ distributions for β_1AR(C163-R1/C344-R1) in DDM and large MSP1D3E1 nanodiscs are displayed in Fig. 4. Addition of ~10 mM CHS to β_1AR (at a CHS-to-β_1AR ratio of 1:700) in DDM micelles results in a ~threefold reduction in the intensity of the intersubunit 26 Å peak (Fig. 4*A*) (29), corresponding to a reduction in dimer from ~17% to ~6% (Table 2). Similar findings are observed for β_1AR reconstituted in MSP1E3D1 nanodiscs: At a CHS-to-β_1AR ratio of 100:1, the intensity of the 26 Å peak is significantly reduced corresponding to a ~fourfold reduction in dimer from ~60 to ~15% (Fig. 4*B* and Table 2); and at a CHS-to-β_1AR ratio of 700:1, the intersubunit 26 Å peak is no longer observable indicating that the reconstituted β_1AR is entirely monomeric under these conditions (Fig. 4*C* and Table 2).

These findings demonstrate that CHS disrupts β_1AR dimer formation in both DDM micelles and lipid nanodiscs through direct interaction of CHS with β_1AR and/or alteration of the physical properties of the lipid micelles and membrane bilayers. CHS, like cholesterol, integrates into lipid bilayers with its hydrophobic steroid core parallel to the lipid acyl chains and its hydrophilic headgroup oriented toward the membrane surface, resulting in an increase in bilayer thickness, a reduction in fluidity and a consequent alteration in membrane geometry (41, 45, 46). CHS aligns with the nanodisc DMPC lipid bilayer in the same manner, thereby permitting CHS to both bind directly to β_1AR and modulate the physical properties of the bilayer.

Single-Molecule Fluorescence Brightness Measurements. As a complementary strategy to probe β_1AR dimerization in nanodiscs, we sought to differentiate dimers and monomers from their fluorescent brightness at the single-molecule level. For this purpose, we labeled β_1AR with Cy3 dyes. Cy3 is covalently linked to cysteine residues via a maleimide-thiol coupling (47), analogous to the MTSL labeling approach used for the DEER measurements, and thus targets the same sites on β_1AR, namely Cys163 and Cys344. Given the two possible labeling positions on β_1AR (Cys163 and Cys344) (Fig. 5*A*), a monomeric receptor can have a maximum single-molecule brightness that corresponds to two Cy3 dyes, while a β_1AR dimer is expected to be twice as bright, with a maximum possible brightness that corresponds to four Cy3 dyes (Fig. 6*A*). In practice, due to incomplete labeling and photobleaching, brightness values may be lower than the maximum allowed by labeling sites, but single molecules with >2 times the Cy3 brightness can be unambiguously identified as dimers.

Single-molecule brightness measurements were conducted using the ABEL trap platform (Fig. 5*B*). The experiments were carried out in solution at room temperature with ultralow concentrations (~20 pM) of Cy3-labeled β_1AR. At such a low concentration in aqueous buffer, individual receptor molecules can randomly diffuse into a ~3 × 3 μm^2 area and be captured for multiple seconds by way of electrokinetic feedback flows (27). During this seconds-long observation window, the single molecule experiences a uniform excitation profile and its brightness can be accurately determined (48).

We first carried out single-molecule brightness measurements on Cy3-β_1AR in DDM. A typical single-molecule trace is shown in Fig. 5*C*. Here, two receptor molecules, solubilized in DDM micelles are captured for seconds long. The first molecule (from 0 to 3.1 s) has an initial brightness of ~180 counts/5 ms, which persists for ~0.8 s before a sudden transition to a lower brightness of ~105

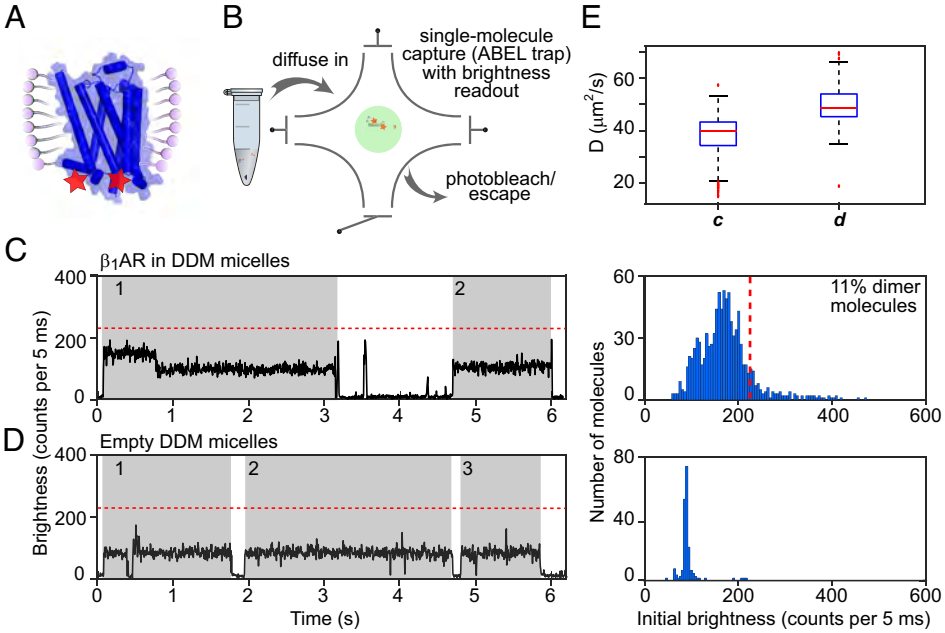

Fig. 5. Probing β_1AR dimerization in DDM micelles using single-molecule brightness measurements. (*A*) Diagrammatic representation of the structure of monomeric β_1AR in DDM micelles with the locations of the Cy3 fluorescent labels at Cys163 and Cys344 shown as red stars. (*B*) Schematic representation of the ABEL trap measurement principle. Example time traces (*Left*) and histograms of initial brightness (*Right*) of control measurements on (*C*) DDM solubilized Cy3-β_1AR (540 molecules) and (*D*) empty DDM micelles (169 molecules). The threshold for identifying a dimer is set at a brightness value of 225 counts/5 ms, indicated by the red dashed lines in both the time trace and histogram panels. The percentage dimer indicated in each histogram is calculated based on this threshold brightness. The lifetime of a molecule containing a single Cy3-β_1AR (one or two Cy3 labels) is marked with a gray background. (*E*) Diffusion coefficients derived from single-molecule ABEL trap measurements; positions ***c*** and ***d*** correspond to the traces in panels (*C*) and (*D*), respectively. In each box, the central mark indicates the median, and the bottom and top edges of the box indicate the 25th and 75th percentiles, respectively. The whiskers extend to the most extreme data points not considered outliers, and the outliers are plotted individually using the "+" marker symbol.

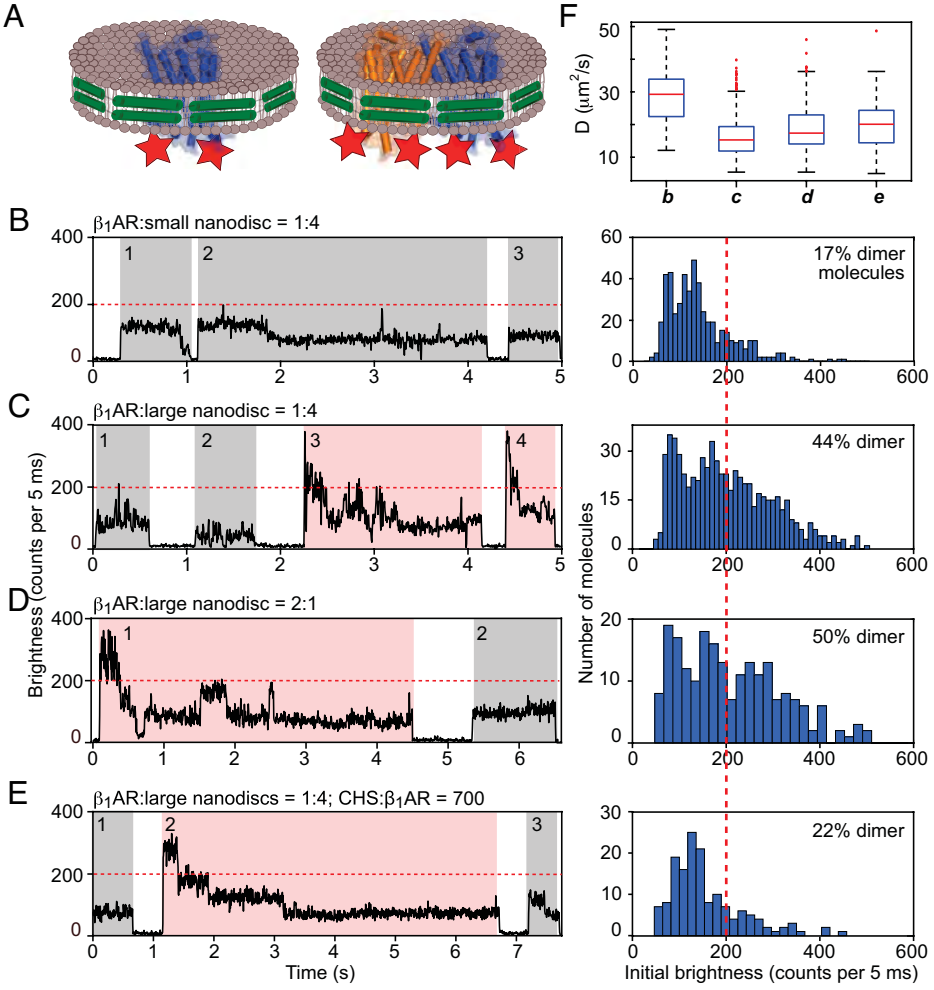

Fig. 6. Probing β_1AR dimerization in nanodiscs using single-molecule brightness measurements. (*A*) Schematic representation of monomeric and dimeric β_1AR incorporated into nanodiscs, with the locations of the Cy3 fluorescent labels at Cys163 and Cys344 shown as red stars. Example time traces (*Left*) and histograms of initial brightness (*Right*) of β_1AR in (*B*) small (9.2 nm) MSP1D1 nanodiscs with a β_1AR-to-nanodisc ratio of 1:4 (502 molecules), (*C*) large (12.5 nm) MSP1E3D1 nanodiscs with a β_1AR-to-nanodisc ratio of 1:4 (664 molecules), (*D*) large MSP1E3D1 nanodiscs with a β_1AR-to-nanodisc ratio of 2:1 (218 molecules), and (*E*) CHS-enriched large MSP1E3D1 nanodiscs with a β_1AR-to-nanodisc ratio of 1:4, where CHS was dissolved in DDM prior to nanodisc reconstruction and added at a β_1AR-to-CHS ratio of 1:700 (152 molecules). The threshold for identifying a dimer is set at a brightness value of 200 counts/5 ms which corresponds to 2.5 Cy3 labels and is indicated by the red dashed lines in both the time trace and histogram panels. The percentage dimer, indicated in each histogram, is calculated based on this threshold brightness. The lifetime of a molecule containing a single Cy3-β_1AR in a nanodisc is delineated by the gray background, while the lifetime of a molecule containing two Cy3-β_1AR in a nanodisc (dimer) is highlighted by the pink background. (*F*) Diffusion coefficients derived from single-molecule ABEL trap measurements; positions ***b–e*** correspond to the traces in panels (*B–E*), respectively. In each box, the central mark indicates the median, and the bottom and top edges of the box indicate the 25th and 75th percentiles, respectively. The whiskers extend to the most extreme data points not considered outliers, and the outliers are plotted individually using the + marker symbol.

counts/5 ms. The lower brightness level subsequently lasts until the 3.1 s mark before a sharp decrease into background. The second molecule shows a single brightness level, similar to the lower brightness level of the first molecule, from start to the end. We interpret the first receptor molecule in the frame to contain two Cy3 dyes which photobleached sequentially and the second receptor molecule to contain only one Cy3 dye. Note that the observed two photobleaching steps are not identical in this case and we attribute this observation to the nonidentical chemical environment of the two labeled cysteine sites on β_1AR, when solubilized in DDM micelles. Collecting data from 540 molecules yields an initial brightness histogram shown in Fig. 5*C* right, where a major peak at ~180 counts/5 ms and minor peak at ~105 counts/5 ms can be identified. We note that the two peaks in the histogram are broad, potentially reflecting the chemical heterogeneity of the two labeling sites and their respective chemical environment. Nevertheless, very few molecules show an initial brightness that is much higher. If we use a threshold of 225 counts/5 ms (which corresponds to the average brightness of 2.5 Cy3 in this experiment) and assign all molecules that exceed the threshold to be β_1AR dimers, we estimate a dimer fraction of ~11%.

Serendipitously, we found that the Cy3 dye can be incorporated nonspecifically into a small fraction (~1%) of empty DDM micelles in the absence of receptors. These Cy3-incorporated empty micelles cannot be pulled down by the nickel column and are absent in the Cy3-β_1AR sample but can serve as a useful control for our methodology. Interestingly, these empty DDM micelles show remarkable homogeneity in their single-molecule brightness profiles: Each molecule displays a single brightness and one-step bleaching (Fig. 5*D*). The brightness histogram from 169 molecules gives a sharp peak at 95 counts/5 ms, which corresponds to a single Cy3 molecule in a homogeneous micelle environment. This control experiment further strengthens our assignment of the labeling stoichiometry and the presence of chemical heterogeneity around the labeling sites in the Cy3-β_1AR experiment.

In addition to accurate brightness measurements, the ABEL trap also determines the diffusion coefficient (*D*) of individual captured molecules. The diffusion information is obtained from statistical

analysis of the feedback voltage time series needed to counteract Brownian motion (27) and reflects the hydrodynamic radius of single molecules. Here, we measured the averaged diffusion coefficient of an empty DDM micelle to be ~50 $\mu m^2/s$ (Fig. 5*E*), which corresponds to a hydrodynamic radius (R_h) of ~4 nm, consistent with previous measurements by dynamic light scattering (R_h ~ 3.5 nm) (49). For the Cy3-β_1AR sample in DDM, $<D>$ ~ 40 $\mu m^2/s$ corresponding to R_h ~ 5 nm. We attribute the ~25% increase in R_h to the incorporation of a Cy3-β_1AR monomer in a DDM micelle.

A typical single-molecule trace for Cy3-β_1AR reconstituted in small MSP1D1 nanodiscs is shown in Fig. 6 *B*, *Left*. Here, we identify three molecules: the first two molecules have similar initial brightness of ~160 counts/5 ms. The second molecule (from 1.1 to 4.2 s) bleached down via an intermediate brightness level at ~80 counts/5 ms. The third molecule showed a single flat brightness level of ~80 counts/5 ms before bleaching. Given that the level at 80 counts/5 ms is the smallest digital step before photobleaching, we identified it to be the brightness of a single Cy3 label in this experiment. Thus, the three receptors in the frame contain 2, 2, and 1 Cy3 dyes, respectively, and all three are identified as β_1AR monomers. Compared to the experiment done in DDM micelles (Fig. 5*C*), the brightness profile has a similar shape with two broad peaks that correspond to one and two Cy3 dyes per receptor. The dye brightness, however, is slightly reduced (80 counts/5 ms here versus 105 counts/5 ms for a single Cy3 from β_1AR in DDM, versus 95 counts/5 ms from empty DDM micelles) and the two Cy3 dyes have equal brightness. These observations may reflect the subtle differences in the local chemical environment as a result of the different solubilization strategies (nanodisc vs DDM micelles). Nevertheless, there are also molecules with much higher brightness and more complicated bleaching dynamics and those are identified as β_1AR dimers. After histogramming all 502 receptors measured ($<D>$ ~ 30 $\mu m^2/s$; Fig. 6*F*) and using 200 counts/5 ms (which corresponds to 2.5 Cy3 labels in this case) as the brightness threshold, we find ~17% of the measured receptors are dimer molecules (Fig. 6 *B*, *Right* panel, and Table 2). Repeating the measurement on Cy3-β_1AR in the large MSP1E3D1 nanodiscs ($<D>$ ~ 16 to 18 $\mu m^2/s$; Fig. 6*F*) reveals a different picture (Fig. 6 *C* and *D*). At a β_1AR-to-nanodisc ratio of 1:4, ~44% of single-molecule traces (664 molecules) exhibited an initial brightness above 200 counts/5 ms, which we attribute to receptor dimers (Fig. 6*C* and Table 2). Increasing the ratio to 2:1 (218 molecules) further raised the dimer fraction by ~6%, reaching a total of ~50% dimer molecules (Fig. 6*D* and Table 2). Both β_1AR-to-nanodisc ratios (1:4 and 2:1) also show complex bleaching dynamics, which could be due to self-quenching between Cy3 dyes brought into close proximity after dimer formation.

Finally, we investigated the effect of CHS on β_1AR dimerization using single-molecule measurements. Unlike DEER, single-molecule brightness analysis does not differentiate between biologically relevant parallel dimers and nanodiscs that are randomly occupied by two monomers which may or may not form antiparallel dimers of no biological relevance. Therefore, we selected a β_1AR-to-nanodisc ratio of 1:4 to minimize stochastic co-occupancy and enable a more direct comparison with the DEER results. Fig. 6*E* shows a significantly lower percentage of identified dimers (~22% dimer molecules) upon addition of CHS, fully consistent with the results from DEER (Fig. 4 and Table 2).

Concluding Remarks. Despite extensive structural studies on GPCRs, the oligomerization behavior of class A GPCRs, such as β_1AR, has remained elusive (4–7). In the current work we investigated β_1AR dimerization using two complementary biophysical methods: pulsed Q-band DEER spectroscopy and single-molecule fluorescence brightness measurements. DEER directly probes long-range distances between site-specific spin labels, making it particularly sensitive for the detection of stable, symmetric parallel dimers (29), and specifically to the dimer formed by transmembrane helices TM1 and TM2 and the C-terminal helix H8 (36) (Fig. 2*B*) that corresponds to the rhodopsin dimer (19). In contrast, single-molecule fluorescence brightness analysis reflects the number of fluorescent labels per particle and can therefore potentially detect both parallel dimers as well as multiple β_1AR monomers incorporated in random orientations (which may include nonbiologically relevant antiparallel dimers) within a nanodisc. Further, in the ABEL trap, the fraction dimeric species is likely underestimated due to incomplete labeling and/or premature photobleaching (where some molecules bleach partially before the observation begins).

Both DEER and single-molecule fluorescence brightness consistently demonstrated that β_1AR is largely monomeric in DDM micelles, while incorporation into lipid nanodiscs preferentially favors β_1AR dimers. In addition, the DEER data indicate that the dimers incorporated into nanodiscs are symmetric with the subunits oriented parallel to one another in the configuration corresponding to the rhodopsin dimer (Fig. 2*B*). Both methods also revealed a clear increase in dimerization upon increasing the size of the nanodiscs. Thus, the larger (12.5 nm) MSP1E3D1 nanodiscs show a significantly higher dimer fraction than the smaller (9.2 nm) MSP1D1 nanodiscs. Quantitatively, at a β_1AR-to-nanodisc ratio of 1:4, DEER spectroscopy provided estimates of the dimer molecule fractions of ~30% in small nanodiscs and ~65% in large nanodiscs. Very similar results were obtained from single-molecule fluorescence brightness experiments with ~17% and ~44% dimer molecules in small and large nanodiscs, respectively, at the same β_1AR-to-nanodisc ratio (Table 2). Given that the values obtained by single-molecule brightness measurements represent lower bounds for the fraction dimer, the agreement between the DEER and single-molecule measurements is remarkably good and would also indicate that the only dimer species incorporated into nanodiscs is the biologically relevant parallel configuration (corresponding to that shown in Fig. 2*B*). We should also note that the dimer fraction determined from the single-molecule measurements is based on a brightness threshold set at 2.5 Cy3 dyes, corresponding to 200 counts/5 ms (Figs. 5 and 6). If this threshold were adjusted to a stricter cutoff of exactly 2 Cy3 dyes, corresponding to ~160 counts/5 ms, the absolute dimer percentage would be increased somewhat. However, the observed trend—namely, that dimerization increases with nanodisc size—remains robust regardless of threshold.

It is important to note that incorporation of β_1AR into nanodiscs reflects a nonequilibrium process: Receptors that fail to transfer from DDM into nanodiscs are lost by precipitation, and thus the resulting sample reflects a selectively stabilized population. Our data indicate that parallel β_1AR dimers are preferentially incorporated into nanodiscs. Thus, even under conditions of a ten-fold molar excess of large nanodiscs relative to β_1AR, the fraction of dimer is significantly enriched in nanodiscs (~44%) relative to DDM micelles (~17%), highlighting the strong influence of the membrane environment on β_1AR oligomerization.

The lack of previous reports on β_1AR dimerization may be attributed to limitations of the systems and methods traditionally used. Most studies have relied on detergent micelles, which, while effective for solubilization, fail to provide the lateral pressure and bilayer architecture necessary to stabilize protein–protein interactions within the membrane. Further, bulk biophysical techniques may not be sensitive enough to detect small dimer populations or may average out transient or heterogeneous states.

Our findings highlight the critical importance of membrane context and experimental resolution in detecting GPCR oligomers. Demonstrating that β_1AR possesses an intrinsic predisposition to form symmetric parallel dimers when a sufficient lipid bilayer environment is present has important implications. In particular, our results suggest that dimerization may be a regulated feature of β_1AR function, potentially influencing receptor signaling, trafficking, and/or pharmacological properties. These insights could potentially guide the design of future functional studies and may possibly be leveraged for therapeutic strategies targeting dimer-specific states.

Experimental Procedures

β_1AR Expression and Purification. Thermostabilized turkey β_1AR was expressed and purified in *Escherichia coli* Rosetta (DE3) competent cells (Sigma Aldrich) as described previously (34). Unless otherwise stated, all purification steps were performed at 4 °C. Purification comprised the following steps (29): solubilization of β_1AR with 1.5% *n*-docecyl-β-D-maltoside (DDM), 0.7% CHAPS [(3-((3-cholamidopropyl) dimethylammonio)-1-propanesulfonate)] and 0.15 % CHS; Ni^{2+}-nitrilotriacetic acid (NTA) affinity chromatography using a 50% Ni agarose resin (ThermoFisher); cleavage of thioredoxin 1 (TrxA) and maltose-binding protein (MBP) fusion tags with human rhinovirus (HRV) 3C protease (ThermoFisher); separation of β_1AR by Sepharose Fast Flow cation exchange (Cytiva) chromatography; further purification with receptor specific alprenolol agarose affinity chromatography (Cube Biotech); and finally Superdex 200 Increase (Cytiva) size exclusion chromatography. The fractions from the final column were analyzed by sodium dodecylsulfate-polyacrylamide gel electrophoresis (SDS-PAGE), and the molecular mass of purified β_1AR was confirmed by matrix assisted laser desorption/ionization (MALDI) mass spectrometry (29). Finally, purified β_1AR was concentrated using a centrifugal concentrator with a molecular weight cutoff of 50,000 (VivaSpin20, Sartorius, Germany) (29).

Expression and Purification of MSP. pET-28a vectors containing MSP1D1 and MSP1E3D1 gene constructs (Addgene) were transformed into T7 Express competent *E. coli* cells (New England Biolabs). Expression and purification were performed as described previously (50). 1 L of Luria–Bertani (LB) broth supplemented with 50 μg/mL kanamycin was grown at 37 °C until the OD_{600} reached 0.6. Protein expression was then induced by adding 1 mM isopropyl β-D-1-thiogalactopyranoside (IPTG), and the cells were grown for a further 2.5 h. Next, the cells were harvested by centrifugation and resuspended in lysis buffer comprising 20 mM Tris pH 7.4, 1% Triton X-100, 1 mM ethylenediaminetetraacetic acid (EDTA) and two tablets of cOmplete™ protease inhibitor cocktail. After sonication, the lysate was cleared by centrifugation and applied to a Ni-NTA agarose resin (Cytiva). The column was washed sequentially with: 1) 40 mM Tris pH 8.0, 300 mM NaCl, and 1% Triton X-100; 2) 40 mM Tris pH 8.0 and 300 mM NaCl, 50 mM cholate and 20 mM imidazole; and 3) 40 mM Tris pH 8.0, 300 mM NaCl, 50 mM imidazole. MSPs were eluted with 40 mM Tris pH 8.0, 300 mM NaCl, and 300 mM imidazole, and dialyzed overnight against 40 mM Tris pH 8.0 and 100 mM NaCl in 10 kDa molecular weight cutoff dialysis tubing. Subsequently, MSPs were incubated at a 1:100 ratio (w/w) of Tobacco Etch Virus (TEV) protease to MSP overnight at 4 °C. The mixture was reloaded onto a Ni-NTA column, and the flow-through containing cleaved MSPs was collected. Finally, the purified MSPs were concentrated to 1 mM, aliquoted, and flash-frozen for future use.

Reconstruction of β_1AR in Nanodiscs. Dimyristoylphosphatidylcholine (DMPC) lipids (Avanti Polar Lipids) were first dissolved in chloroform and then evaporated to remove the solvent. The dried lipid film was subsequently dissolved in 100 mM sodium cholate (Sigma-Aldrich) to obtain a final 50 mM stock solution. For β_1AR-containing nanodiscs, purified β_1AR (~60 μM) in a DDM-containing buffer was mixed with MSP and DMPC/cholate at the ratios specified in Table 1. The concentration of cholate was kept to at least 14 mM for all samples. After 1 h incubation at 25 °C, BioBeads SM-2 resin (Bio-Rad), prewashed with methanol, water, and nanodisc buffer (50 mM Tris pH 8.0 and, 300 mM NaCl), was added. The mixture was incubated at 25 °C for another 1 h, and then placed at 4 °C overnight to remove residual DDM. The following day, BioBeads were removed, and the mixture was filtered through ultracentrifugal filters (Sigma-Aldrich) before being applied to a His-Ni-sepharose column (Cytiva). Empty nanodiscs elute directly in the flow-through, while β_1AR-containing nanodiscs were eluted with 500 mM imidazole. Finally, the β_1AR-containing nanodiscs were purified by gel filtration on a Superdex 200 Increase 10/300 GL column in 40 mM Tris pH 8.0 and 300 mM NaCl, at a flow rate of 1 mL/min and 25 °C.

β_1AR Nitroxide Spin Labeling for DEER Experiments. R1 nitroxide labeling of β_1AR was carried out prior to nanodisc reconstruction using S-(1-oxyl-2,2,5,5-tetramethyl-2,5-dihydro-1H-pyrrol-3-yl) methyl methane sulfonothioate (MTSL; Toronto Research Chemicals), as previously described (29). Briefly, a ten-fold molar excess of MTSL was added to β_1AR (~60 μM), followed by 2 h incubation at room temperature and an additional 12 h incubation at 4 °C. Excess spin label was then removed by multiple washes in centrifugal concentrator. The spin-labeled β_1AR sample was subsequently used for β_1AR-containing nanodisc reconstruction, following the protocol described above. For flash-freezing, 15 μL of R1-labeled β_1AR in nanodiscs in buffer (40 mM Tris pH 8.0 and 300 mM NaCl) containing 30% (v/v) d_8-glycerol was placed into EPR tubes (1 mm inner diameter, 1.6 mm outer diameter; VitroCom) and plunged directly into liquid nitrogen.

Q-Band DEER. Pulsed EPR DEER data were collected at Q-band (33.8 GHz) at a temperature of 50 K on a Bruker E-580 spectrometer equipped with a 150 W traveling-wave tube amplifier, a model ER5107D2 resonator, and a cryo-free cooling unit, as described previously (51). Four-pulse DEER experiments were acquired using a conventional four-pulse sequence (25). The observer and electron–electron double resonance (ELDOR) pump pulses were separated by about 80 MHz, with the observer π/2 and π pulses set to 12 and 24 ns, respectively, and the ELDOR π pulse set to 10 ns; the pump frequency was centered at the Q-band nitroxide spectrum located at +40 MHz from the center of the resonator frequency; the τ_1 value of 400 ns for the first echo-period time was incremented eight times in 16 ns steps to average ^{2}H modulation; and the position of the ELDOR pump pulse was incremented in steps of Δt = 4 ns. The bandwidth of the overcoupled resonator was 120 MHz (29). All DEER echo curves were acquired for t_{max} = 2.5 μs with the total length ($T = 2\tau_2$) of the dipolar evolution time set to 6 μs; data collection was not extended to the full τ_2 (3 μs) range because of a "2 + 1" echo perturbation of the DEER echo curves at a time of about t_1 from the final observe π pulse (29). Each DEER echo curve was averaged for ~12 h with a shot repetition time of 6 ms. The pulse gate time used for echo integration was 32 ns.

All the raw DEER data have been deposited in FigShare (https://doi.org/10.6084/m9.figshare.29877635) (52).

***P*(*r*) Distributions from DEER Echo Curves.** $P(r)$ pairwise distributions were obtained from the DEER echo curves using model-free validated Tikhonov regularization as implemented in the program DeerLab (40), with bootstrap analysis for uncertainty quantification via the bootan function in the DeerLab library and the number of bootstrap samples evaluated set to 1,000 (29). In addition, compactness regularization was imposed upon the distance distribution, as described in ref. 53. The DeerLab processing script is provided in *SI Appendix*.

β_1AR Fluorophore Labeling for Single-Molecule Fluorescence Brightness Experiments. Fluorophore labeling was carried out in a similar manner to nitroxide spin labeling, except that Cy3-maleimide (Lumiprobe 11080) was used instead of MTSL. The labeling reaction was conducted at room temperature for 1 h and subsequently purified using a size-exclusion column (p6, Biorad) followed by a His-Ni-sepharose column (Cytiva) in 20 mM Tris pH 7.5, 350 mM NaCl, and 0.15% DDM. β_1AR was eluted with 250 mM imidazole. We note that Cy3 has a tendency to be nonspecifically incorporated into micelles and the Ni column step was essential to isolate Cy3 labeled receptors. The averaged degree of labeling was 0.8 Cy3 per site (i.e. at C163 and C344). The Cy3 labeled β_1AR was subsequently reconstituted into nanodiscs following the procedures described in *Reconstruction of β_1AR in Nanodiscs*.

Single-Molecule Brightness Measurements. Measurement of single-molecule brightness was conducted in a custom-built ABEL trap instrument as previously published (54), using a 532 nm excitation laser. Experiments with nanodiscs were conducted in 20 mM HEPES pH 7.8 and 100 mM NaCl at a concentration of ~20 pM labeled β_1AR receptors. About 150 to 600 molecules were collected for each sample condition. Single-molecule traces typically show step-wise bleaching and/or complex dynamics during the observation window. As an attempt to accurately count the number of Cy3 labels attached to the β_1AR receptor, we calculated the "initial brightness" as the average brightness from the start of the trace until any brightness drop, as identified by a change point algorithm (55).

Data, Materials, and Software Availability. All the raw DEER data have been deposited in FigShare (https://doi.org/10.6084/m9.figshare.29877635) (52). All other data are included in the article and/or *SI Appendix*.

ACKNOWLEDGMENTS. We thank Drs. Stefan Grzesiek and Marco Rogowski for providing the β_1AR plasmid, and Dr Rodolfo Ghirlando for extensive discussions. This work was supported by the Intramural Program of the National Institute of Diabetes and Digestive and Kidney Diseases, NIH (DK-029023 to G.M.C. and DK-057171 to Q.W.). The contributions of the NIH authors were made as part of their official duties as NIH Federal employees, are in compliance with agency policy requirements, and are considered Works of the United States Government. However, the findings and conclusions presented in this paper are those of the authors and do not necessarily reflect the views of the NIH or the U.S. Department of Health and Human Services.

Author affiliations: [a]Laboratory of Chemical Physics, National Institute of Diabetes and Digestive and Kidney Diseases, National Institutes of Health, Bethesda, MD 20892-0520

1. D. M. Rosenbaum, S. G. Rasmussen, B. K. Kobilka, The structure and function of G protein-coupled receptors. *Nature* **459**, 356–363 (2009).
2. I. Shimada, T. Ueda, Y. Kofuku, M. T. Eddy, K. Wuthrich, GPCR drug discovery: Integrating solution NMR data with crystal and cryo-EM structures. *Nat. Rev. Drug Discov.* **18**, 59–82 (2019).
3. M. Zhang *et al.*, G protein-coupled receptors (GPCRs): Advances in structures, mechanisms, and drug discovery. *Signal Transduct. Target. Ther.* **9**, 88 (2024).
4. V. V. Gurevich, E. V. Gurevich, How and why do GPCRs dimerize? *Trends Pharmacol. Sci.* **29**, 234–240 (2008).
5. K. Palczewski, Oligomeric forms of G protein-coupled receptors (GPCRs). *Trends Biochem. Sci.* **35**, 595–600 (2010).
6. P. M. Dijkman *et al.*, Dynamic tuneable G protein-coupled receptor monomer-dimer populations. *Nat. Commun.* **9**, 1710 (2018).
7. A. Gusach, J. Garcia-Nafria, C. G. Tate, New insights into GPCR coupling and dimerisation from cryo-EM structures. *Curr. Opin. Struct. Biol.* **80**, 102574 (2023).
8. H. Guo *et al.*, Methods used to study the oligomeric structure of G-protein-coupled receptors. *Biosci. Rep.* **37**, BSR20160547 (2017).
9. V. V. Gurevich, E. V. Gurevich, GPCR monomers and oligomers: It takes all kinds. *Trends Neurosci.* **31**, 74–81 (2008).
10. M. Mohole, G. A. Kumar, D. Sengupta, A. Chattopadhyay, "Molecular determinants of GPCR oligomerization" in *GPCRs: Structure, Function and Drug Discovery*, B. Jastrzebska, P.S.-H. Park, Eds. (Elsevier, 2019).
11. E. Serebryany, G. A. Zhu, E. C. Yan, Artificial membrane-like environments for in vitro studies of purified G-protein coupled receptors. *Biochim. Biophys. Acta* **1818**, 225–233 (2012).
12. I. G. Denisov, Y. V. Grinkova, A. A. Lazarides, S. G. Sligar, Directed self-assembly of monodisperse phospholipid bilayer nanodiscs with controlled size. *J. Am. Chem. Soc.* **126**, 3477–3487 (2004).
13. T. H. Bayburt, Y. V. Grinkova, S. G. Sligar, Assembly of single bacteriorhodopsin trimers in bilayer nanodiscs. *Arch. Biochem. Biophys.* **450**, 215–222 (2006).
14. K. Palczewski *et al.*, Crystal structure of rhodopsin: A G protein-coupled receptor. *Science* **289**, 739–745 (2000).
15. T. H. Bayburt, A. J. Leitz, G. Xie, D. D. Oprian, S. G. Sligar, Transducin activation by nanoscale lipid bilayers containing one and two rhodopsins. *J. Biol. Chem.* **282**, 14875–14881 (2007).
16. G. M. Hu, T. L. Mai, C. M. Chen, Visualizing the GPCR network: Classification and evolution. *Sci. Rep.* **7**, 15495 (2017).
17. L. Hein, B. K. Kobilka, Adrenergic receptors from molecular structure to in vivo function. *Trends Cardiovasc. Med.* **7**, 137–145 (1997).
18. A. Mahmood, K. Ahmed, Y. Zhang, **B**-adrenergic receptor desensitization/down-regulation in heart failure: A friend or foe? *Front. Cardiovasc. Med.* **9**, 925692 (2022).
19. D. Fotiadis *et al.*, The G protein-coupled receptor rhodopsin in the native membrane. *FEBS Lett.* **564**, 281–288 (2004).
20. D. Y. Zhao *et al.*, Cryo-EM structure of the native rhodopsin dimer in nanodiscs. *J. Biol. Chem.* **294**, 14215–14230 (2019).
21. S. Angers *et al.*, Detection of β_2-adrenergic receptor dimerization in living cells using bioluminescence resonance energy transfer (BRET). *Proc. Natl. Acad. Sci. U.S.A.* **97**, 3684–3689 (2000).
22. J. F. Mercier, A. Salahpour, S. Angers, A. Breit, M. Bouvier, Quantitative assessment of β_1- and β_2-adrenergic receptor homo- and heterodimerization by bioluminescence resonance energy transfer. *J. Biol. Chem.* **277**, 44925–44931 (2002).
23. C. Lavoie *et al.*, S_1/ β_2-adrenergic receptor heterodimerization regulates β_2-adrenergic receptor internalization and erk signaling efficacy. *J. Biol. Chem.* **277**, 35402–35410 (2002).
24. L. A. Devi, G-protein-coupled receptor dimers in the lime light. *Trends Pharmacol. Sci.* **21**, 324–326 (2000).
25. M. Pannier, S. Veit, A. Godt, G. Jeschke, H. W. Spiess, Dead-time free measurement of dipole–dipole interactions between electron spins. *J. Magn. Reson.* **142**, 331–340 (2000).
26. G. Jeschke, Deer distance measurements on proteins. *Annu. Rev. Phys. Chem.* **63**, 419–446 (2012).
27. Q. Wang, R. H. Goldsmith, Y. Jiang, S. D. Bockenhauer, W. E. Moerner, Probing single biomolecules in solution using the anti-brownian electrokinetic (ABEL) trap. *Acc. Chem. Res.* **45**, 1955–1964 (2012).
28. Q. Wang, W. E. Moerner, Lifetime and spectrally resolved characterization of the photodynamics of single fluorophores in solution using the anti-Brownian electrokinetic trap. *J. Phys. Chem. B.* **117**, 4641–4648 (2013).
29. N. Kubatova, T. Schmidt, C. D. Schwieters, G. M. Clore, Quantitative analysis of sterol-modulated monomer-dimer equilibrium of the β1-adrenergic receptor by DEER spectroscopy. *Proc. Natl. Acad. Sci. U.S.A.* **120**, e2221036120 (2023).
30. J. M. Hutchison *et al.*, Dodecyl-β-melibioside detergent micelles as a medium for membrane proteins. *Biochemistry* **56**, 5481–5484 (2017).
31. M. Ehsan *et al.*, Steroid-based amphiphiles for membrane protein study: The importance of alkyl spacers for protein stability. *Chembiochem* **19**, 1433–1443 (2018).
32. S. G. Sligar, I. G. Denisov, Nanodiscs: A toolkit for membrane protein science. *Protein Sci.* **30**, 297–315 (2021).
33. M. Zhang *et al.*, Cryo-EM structure of an activated GPCR-G protein complex in lipid nanodiscs. *Nat. Struct. Mol. Biol.* **28**, 258–267 (2021).
34. L. A. Abiko, M. Rogowski, A. Gautier, G. Schertler, S. Grzesiek, Efficient production of a functional G protein-coupled receptor in *E. coli* for structural studies. *J. Biomol. NMR* **75**, 25–38 (2021).
35. T. Schmidt, N. Kubatova, G. M. Clore, Deconvoluting monomer- and dimer-specific distance distributions between spin labels in a monomer/dimer mixture using T_1-edited DEER EPR spectroscopy. *J. Am. Chem. Soc.* **146**, 17964–17973 (2024).
36. J. Huang, S. Chen, J. J. Zhang, X. Y. Huang, Crystal structure of oligomeric β_1-adrenergic G protein-coupled receptors in ligand-free basal state. *Nat. Struct. Mol. Biol.* **20**, 419–425 (2013).
37. J. L. Baber, J. M. Louis, G. M. Clore, Dependence of distance distributions derived from double electron–electron resonance pulsed EPR spectroscopy on pulse-sequence time. *Angew. Chem. Int. Ed. Engl.* **54**, 5336–5339 (2015).
38. T. Warne *et al.*, The structural basis for agonist and partial agonist action on a β_1-adrenergic receptor. *Nature* **469**, 241–244 (2011).
39. C. D. Schwieters, G. A. Bermejo, G. M. Clore, Xplor-NIH for molecular structure determination from NMR and other data sources. *Protein Sci.* **27**, 26–40 (2018).
40. L. Fabregas Ibanez, G. Jeschke, S. Stoll, Deerlab: A comprehensive software package for analyzing dipolar electron paramagnetic resonance spectroscopy data. *Magn. Reson. (Gott.)* **1**, 209–224 (2020).
41. A. Rosenhouse-Dantsker, A. N. Bukiya, "Cholesterol modulation of protein function" in *Advances in Experimental Medicine and Biology*, A. Rosenhouse-Dantsker, A. N. Bukiya, Eds. (Springer, 2019), vol. 1115.
42. P. Sarkar, A. Chattopadhyay, Cholesterol in GPCR structures: Prevalence and relevance. *J. Membr. Biol.* **255**, 99–106 (2022).

43. L. A. Abiko *et al.*, Filling of a water-free void explains the allosteric regulation of the β_1-adrenergic receptor by cholesterol. *Nat. Chem.* **14**, 1133–1141 (2022).
44. M. A. Hanson *et al.*, A specific cholesterol binding site is established by the 2.8 Å structure of the human β_2-adrenergic receptor. *Structure* **16**, 897–905 (2008).
45. S. T. Yang, A. J. B. Kreutzberger, J. Lee, V. Kiessling, L. K. Tamm, The role of cholesterol in membrane fusion. *Chem. Phys. Lipids* **199**, 136–143 (2016).
46. O. Soubias, A. J. Sodt, W. E. Teague, K. G. Hines, K. Gawrisch, Physiological changes in bilayer thickness induced by cholesterol control GPCR rhodopsin function. *Biophys. J.* **122**, 973–983 (2023).
47. T. Ha, Single-molecule fluorescence resonance energy transfer. *Methods* **25**, 78–86 (2001).
48. Y. Jiang *et al.*, Sensing cooperativity in ATP hydrolysis for single multisubunit enzymes in solution. *Proc. Natl. Acad. Sci. U.S.A.* **108**, 16962–16967 (2011).
49. A. A. Thompson *et al.*, GPCR stabilization using the bicelle-like architecture of mixed sterol-detergent micelles. *Methods* **55**, 310–317 (2011).
50. T. K. Ritchie *et al.*, Reconstitution of membrane proteins in phospholipid bilayer nanodiscs. *Meth. Enzymol.* **464**, 211–231 (2009).
51. T. Schmidt, C. D. Schwieters, G. M. Clore, Spatial domain organization in the HIV-1 reverse transcriptase p66 homodimer precursor probed by double electron-electron resonance EPR. *Proc. Natl. Acad. Sci. U.S.A.* **116**, 17809–17816 (2019).
52. N. Kubatova, T. Schmidt, G. M. Clore, Raw Deer data for the β1-adrenergic receptor in lipid nanodiscs. Figshare. https://doi.org/10.6084/m9.figshare.29877635. Deposited 10 August 2025.
53. L. Fabregas-Ibanez, G. Jeschke, S. Stoll, Compactness regularization in the analysis of dipolar EPR spectroscopy data. *J. Magn. Reson.* **339**, 107218 (2022).
54. H. Wilson, Q. Wang, ABEL-FRET: Tether-free single-molecule FRET with hydrodynamic profiling. *Nat. Methods* **18**, 816–820 (2021).
55. L. P. Watkins, H. Yang, Detection of intensity change points in time-resolved single-molecule measurements. *J. Phys. Chem. B* **109**, 617–628 (2005).